Prospect study for the measurement of the $Hb\bar{b}$ coupling at the LHC and FCC-hh

Zahra Abdy [1] and Mojtaba Mohammadi Najafabadi [2,3]

[1] AGH University of Science and Technology, Faculty of Physics and Applied Computer Science, Aleja Mickiewicza 30, 30-055 Krakow, Poland

[2] Experimental Physics Department, CERN, 1211 Geneva 23, Switzerland

[3] School of Particles and Accelerators, Institute for Research in Fundamental Sciences (IPM), P.O. Box 19395-5531, Tehran, Iran

(Received 22 January 2024; accepted 3 May 2024; published 22 May 2024)

This paper employs the $H + b +$ jets signature in proton-proton collisions to explore the structure of the $Hb\bar{b}$ couplings. The focus of the analysis lies in the decay of the Higgs boson into a photon pair, taking into account both reducible and irreducible backgrounds and a realistic simulation of the detector effects. To enhance the discrimination between signal and background, a multivariate analysis is employed to analyze the kinematic variables and optimise the signal-to-background ratio. The results indicate that the $H + b +$ jets process can significantly contribute to the precise measurement of CP-even and CP-odd couplings between the bottom quark and the Higgs boson at the LHC and FCC-hh. Finally, a novel asymmetry is introduced for the purpose of probing CP violation within the $Hb\bar{b}$ coupling, formulated exclusively based on lab-frame momenta.

DOI: 10.1103/PhysRevD.109.093003

I. INTRODUCTION

The observation of the $H \to b\bar{b}$ decay mode by the ATLAS and CMS experiments has been made through the Higgs boson production in association with a massive vector boson V ($V = W, Z$) processes [1,2]. Both the ATLAS and CMS analyses rely on the leptonic decays of the vector boson ($W^{\pm}$ and Z) for triggering the events and to suppress the QCD multijet background. The most recent measurements for observation of the $H \to b\bar{b}$ via VH processes are presented using the whole Run 2 data collected by the ATLAS experiment in proton-proton collisions with an integrated luminosity of 139 fb^{-1} at $\sqrt{s} = 13$ TeV. For a Higgs boson with 125 GeV produced in either HZ or HW channel, an observed significance of 6.7 standard deviations is obtained from the ATLAS experiment and the measured signal strength relative to the prediction of SM is found to be [3]

$$\mu_{bb} = 1.02 \pm 0.12(\mathrm{stat}) \pm 0.14(\mathrm{syst}), \tag{1}$$

Similar measurement by the CMS experiment is available with a combination of Run 1 data (7 TeV and 8 TeV) and part of Run 2 (2017 data corresponding to an integrated luminosity of 41.3 fb^{-1}). The observed significance of 5.6 standard deviations and the measured signal strength from the combination ZH and WH processes is [2]

$$\mu_{bb} = 1.04 \pm 0.2(\mathrm{stat} \oplus \mathrm{syst}), \tag{2}$$

As can be seen, the overall uncertainty is around 20% in both measurements from the ATLAS and CMS experiments and the results are in agreement with the Standard Model (SM) prediction within the uncertainties. In the future, at the HL-LHC, an improvement of 10% in tagging the b-quark jets efficiency is expected which leads to a relative improvement in the uncertainty of signal strength of up to 4.7% [4].

A global fit of the Higgs boson couplings has been conducted in Ref. [5] utilizing the comprehensive Higgs datasets collected at the LHC, encompassing integrated luminosities per experiment of approximately 5 fb^{-1} at 7 TeV, 20 fb^{-1} at 8 TeV, and up to 139 fb^{-1} at 13 TeV. This analysis included the exploration of CP-even and CP-odd couplings of the Higgs boson to bottom quarks. To probe the Higgs boson coupling with the SM particles and find any deviation from the SM predictions, the κ–framework is used [6]. In this framework, possible deviation for the Higgs-bottom quark coupling is defined by $\kappa_b^2 = \Gamma_{H\to b\bar{b}}/\Gamma^{\mathrm{SM}}_{H\to b\bar{b}}$. The current measurement of κ_b at 68% CL, obtained from a general fit to the Higgs boson couplings, is $0.99^{+0.17}_{-0.16}$ [7]. At HL-LHC, assuming similar systematic uncertainties to the Run 2 of the LHC, κ_b is expected to be measured with an uncertainty of ± 0.042 at 68% CL [8].

Except for some anomalies which are listed in Ref. [9] and references therein, all the experimental results obtained by the LHC experiments are consistent with the SM expectations within the uncertainties. In particular, the measured Higgs boson couplings with the SM fields are in agreement within the total uncertainties [7]. Therefore, any new degree of freedom could be foreseen to be well separated in mass from the SM particles [10,11]. As there are several beyond SM theories, with similar experimental signatures in some cases, an easy and efficient way to search for new physics effects is to rely on a model-independent way. In a model independent approach, the impacts of new physics could show up in an effective field theory (EFT) extension of the SM which consists of an infinite series of effective operators with higher dimensions [12–19]. The leading contributions to the effective extension of the SM originate from the dimension-6 operators that is based on a nonredundant and complete operator basis [20,21]. Not only these operators can modify the signal strengths but also the differential distributions may be affected because of the presence of new vertex structures. Several effective operators are contributing to the Higgs boson couplings with the SM fields which persuade us to pay attention to all possible Higgs involved processes at the colliders. Probing processes where Higgs boson is present such as Higgs boson associated production, H + jets, and various processes where Higgs boson is off-shell provides useful information of the new higher order effective couplings. There are already several studies for investigating the EFT extension of the SM in the Higgs boson sector [22–43].

Higgs boson production in association with a pair of $b\bar{b}$ at hadron colliders ($pp \to H + b + \bar{b}$), has received attention as a direct way to probe both the CP-even and CP-odd structures of the bottom quark Yukawa coupling [44,45]. In Ref. [44], using the kinematic shapes of $\gamma\gamma b\bar{b}$ final state in boosted decision trees, a specific way to achieve a strong sensitivity to bottom quark Yukawa coupling is presented. The analysis has been performed at HL-LHC and Future Circular Collider proton-proton (FCC-hh) considering the main sources of background processes. In conjunction with the HL-LHC, anticipated to operate at a center-of-mass energy of 14 TeV and an integrated luminosity of 3 ab^{-1}, the analysis of Ref. [44] has been extended to the forthcoming FCC-hh facility. This future endeavor is poised to operate at an even higher center-of-mass energy, 100 TeV, coupled with a substantially increased integrated luminosity of 15 ab^{-1} [46]. The inclusion of FCC-hh as the succeeding flagship hadron collider initiative for the CERN, as indicated in the updated European strategy report, underscores its pivotal role in advancing the frontier of particle physics research [47].

In Ref. [45], both a cut-based analysis and a gradient boost algorithm have been exploited to probe bottom quark Yukawa coupling through $Hb\bar{b}$ channel with $4b$ final state. This analysis only focuses on probing the CP-even structure of the $Hb\bar{b}$ coupling. The primary objective of this research paper is to investigate the $H + b + (\mathrm{jet})$ process and its potential to extract the CP-even and CP-odd components of the bottom quark Yukawa coupling within the framework of effective field theory (EFT). The approach employed for this purpose involves utilizing machine learning techniques. The $H + b + (\mathrm{jet})$ process under study allows for the inclusion of either a light-flavor jet or a b-quark jet. The rationale behind exploring this process is twofold. Firstly, by examining the capabilities of the $H + b + (\mathrm{jet})$ process to probe the structure of $Hb\bar{b}$ couplings, a comparative analysis can be performed in relation to other relevant processes. Secondly, the research delves into the efficacy of a multivariate technique that leverages the shapes of the final state to discriminate between the signal and the main SM background processes. Through this investigation, we aim to gain valuable insights into the underlying physics of the $H + b + (\mathrm{jet})$ process and its significance in probing both CP-odd and CP-even $Hb\bar{b}$ couplings. Additionally, we seek to assess the strength of the machine learning-based multivariate approach in effectively distinguishing the signal from the SM background processes.

This paper is organized as follows. The theoretical framework of the $Hb\bar{b}$ effective coupling is described in Sec. II. In Sec. III, we discuss the Higgs production in association with a bottom quark and additional jet. In Sec. IV, the analysis strategy and details of event simulation are explained. The results of the analysis, exemplified for the HL-LHC and for the FCC-hh, are given in Sec. V. An asymmetrylike observable is introduced in Sec. VI to explore the CP-violating term of the $Hb\bar{b}$ coupling. Finally, we summarize and conclude in Sec. VII.

II. THEORETICAL FRAMEWORK

As referenced in the preceding section, this study has been conducted within the framework of the EFT, where manifestations of new physics are anticipated to emerge through novel interactions among the SM fields. In this context, the introduction of new couplings is suppressed by inverse powers of Λ, which serves as the characteristic scale representing physics beyond the SM. In the EFT, the effects of heavy new degrees of freedom are integrated out and the SM gauge symmetries, Lorentz invariance and lepton and baryon number conservation are respected. The new physics effects are parametrized by higher-dimension operators with not-known Wilson coefficients and the main contributions to the observable come from dimension-6 operators. In this work we rely on the Higgs characterization model [48] based on an EFT approach where the $Hf\bar{f}$ interaction has the following form:

$$\mathcal{L}_{Hf\bar{f}} = -\sum_{f=e,\mu,\tau,u,d,c,s,b,t} \frac{y_f^{\mathrm{SM}}}{\sqrt{2}} \bar{f}(c_f + i\tilde{c}_f\gamma_5) f H, \quad (3)$$

where the Higgs boson field is denoted by H and f is the fermion field. The SM Yukawa coupling of a fermion f is shown by coupling y_f^{SM}. Modifications from the dimension six operators to the $Hf\bar{f}$ CP-even and CP-odd couplings show up in c_f and $\tilde{c}_f$ parameters, respectively. In the SM, $c_f = 1.0$ and $\tilde{c}_f = 0.0$ and $y_f^{\mathrm{SM}}/\sqrt{2} = m_f/v$, where v is the vacuum expectation value. Both c_f and $\tilde{c}_f$ for the top and bottom quarks can be indirectly studied through the measured Higgs boson production cross section via gluon-gluon fusion [$\sigma(gg \to H)$] and the decay width of the Higgs boson into two photons [$\Gamma(H \to \gamma\gamma)$]. The modifications that $\Gamma(H \to \gamma\gamma)$ and $\sigma(gg \to H)$ receive only from third quark generation are [23]

$$\begin{aligned} \kappa_\gamma^2 &= 0.08c_t^2 + 0.18\tilde{c}_t^2 + 4\times10^{-5}\times(c_b^2 + \tilde{c}_b^2) \\ &\quad - 0.002\times c_t c_b - 0.004\tilde{c}_t\tilde{c}_b, \\ \kappa_g^2 &= 1.11c_t^2 + 2.56\tilde{c}_t^2 + 0.01\times(c_b^2 + \tilde{c}_b^2) \\ &\quad - 0.12\times c_t c_b - 0.2\tilde{c}_t\tilde{c}_b, \end{aligned} \quad (4)$$

where $\kappa_g = \sigma(gg\to H)/\sigma_{\mathrm{SM}}(gg\to H)$ and $\kappa_\gamma = \Gamma(H\to\gamma\gamma)/\Gamma_{\mathrm{SM}}(H\to\gamma\gamma)$. As can be seen, the gluon fusion cross section can deviate significantly from its SM prediction even with minor deviations of c_t and $\tilde{c}_t$ from their SM values. However, the impact of c_t and $\tilde{c}_t$ on κ_γ is less pronounced. When compared to the top-quark coupling, variations in the coupling modifiers of the bottom quark (c_b and $\tilde{c}_b$) exhibit much smaller magnitudes in κ_g and κ_γ. As discussed in Ref. [23], from Eq. (4), the gluon fusion cross section exhibits an enhancement of approximately 26% when considering a negative value for c_b parameter falling within 2σ allowed region, specifically $-1.23 \le c_b \le -1.08$. Meanwhile, the diphoton decay width experiences a reduction of around 3% within this specified region. On the other hand, the impact of $\tilde{c}_b$ on κ_g and κ_γ remains at the subpercent level and loose limits on $\tilde{c}_b$ could be derived from κ_g and κ_γ [23].

In addition to the gluon fusion Higgs boson cross section and diphoton decay width of the Higgs boson, the CP-odd component of the $Hb\bar{b}$ coupling, $\tilde{c}_b$, can be constrained using the electron electric dipole moment (EDM). This contribution to the EDM of the electron, d_e, occurs through loop processes. Consequently, the value of $\tilde{c}_b$ can be indirectly constrained by considering the existing experimental limit on d_e [43]. The ACME Collaboration has established an experimental limit on the electron EDM at a 90% confidence level to be $|d_e| \le 1.1\times10^{-29}$ e cm [49]. Using this bound on the electron EDM, the constraint on $\tilde{c}_b$ at a 90% CL is found to be $\tilde{c}_b < 0.26$. It is important to note that this limit is derived under the assumption that there are no deviations from the SM in the $He\bar{e}$ coupling and that no cancellations occur with other contributing mechanisms.

As a direct way to probe the $Hb\bar{b}$ interaction, the analysis of $H + b + \bar{b}$ production at the LHC and FCC-hh is expected to provide the following constraints at 1σ [44]:

$$\begin{aligned} &c_b \in [-0.99, -0.82] \cup [0.84, 1.14], \quad \text{at HL-LHC with } 6\ \mathrm{ab}^{-1}, \\ &c_b \in [0.99, 1.01], \quad \text{at FCC-hh with of } 30\ \mathrm{ab}^{-1}. \end{aligned} \quad (5)$$

where the result of HL-LHC and FCC-hh are obtained with an integrated luminosity of 6 ab^{-1} and 30 ab^{-1}, respectively.

III. HIGGS BOSON PRODUCTION ASSOCIATED WITH A BOTTOM QUARK JET AND AN ADDITIONAL JET

In this section, we describe the production of a Higgs boson associated with a b-quark jet and additional jet in proton-proton collisions which occur at the LHC and FCC-hh. In the SM, the $H + b +$ (jet) production proceeds through the gluon-b quark interactions, quark-(anti)quark annihilation, and gluon-gluon fusion. The representative Feynman diagrams are shown in Fig. 1. The filled circles represent the vertices in the diagram that undergo modifications due to the effective interaction of $Hb\bar{b}$ introduced in Eq. (3).

The cross section for $H + b$ processes, involving the production of a Higgs boson and a bottom quark, is of the order of $\mathcal{O}(\alpha_s (y_b^{\mathrm{SM}})^2)$, where y_b^{SM} represents the Yukawa coupling strength of the b-quark and α_s denotes the strong coupling constant. On the other hand, the higher-order processes that include an additional jet have a cross section of $\mathcal{O}(\alpha_s^2 (y_b^{\mathrm{SM}})^2)$. These processes involve the emission of

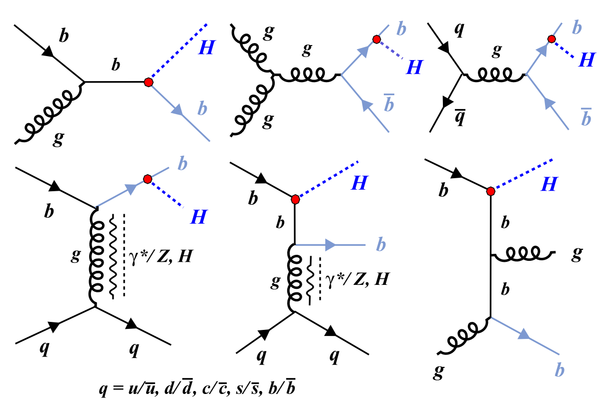

FIG. 1. Representative Feynman diagrams for production of Higgs boson in association with a bottom quark and an additional parton at leading order. The filled red circle presents the effective coupling of the $Hb\bar{b}$.

an extra jet alongside the Higgs boson and bottom quark, resulting in a higher suppression factor due to the additional power of the strong coupling constant.

To gain insights into the impact of varying the coupling modifiers at the LHC, we examine the changes in the signal cross section concerning the SM when c_b is altered by approximately 10% from their SM values. For $c_b = 1.1$, the relative change in the cross section is approximately 18%, whereas for $c_b = 0.9$, $|\Delta\sigma|/\sigma_{\rm SM} = 17\%$. Additionally, the effect of changing $\tilde{c}_b$ within $\pm 20\%$ and $\pm 40\%$ of the SM value, results in relative changes of approximately 3% and 21%, respectively.

To assess the effects of the $Hb\bar{b}$ effective couplings on $Hb(H\bar{b})$ productions in association with a jet, the MadGraph5_aMC@NLO package (version 3.5.1) [50–52] is utilized. This package allows for the calculation of cross sections and event generation for various processes. In this case, the effective Lagrangian, as introduced in Eq. (3), is implemented in the FeynRule program. The resulting model, known as the Universal FeynRules Output (UFO) model [53,54], is then provided as input to the MadGraph5_aMC@NLO program. The production of $Hb/H\bar{b}$ with an additional parton in the final state is considered at leading order, employing relevant matrix elements. The events with zero and one additional parton are combined using the MLM matching scheme [55], which ensures a consistent description of the production process.

In this study, we aim to determine a realistic sensitivity of the $H + b +$ jet process to general $Hb\bar{b}$ coupling, specifically focusing on the c_b and $\tilde{c}_b$. To achieve this, we carry out the analysis using the Higgs decay channel to two photons, which is known for its well-reconstructed and rather clean signature. This choice allows us to well-estimate the background processes and provides valuable insights into the impact of different contributions on c_b and $\tilde{c}_b$. With Higgs boson decaying into two photons, the final state consists of two photons and at least one jet from which at least one is originating from the hadronization of a b-quark.

The analysis considers several dominant background processes that contribute to the signal. These background processes, which need to be carefully taken into account, include:

(i) SM production of $H + b +$ jet (merged $H + b$ and $H + b +$ jet using MLM prescription), where Higgs boson decays into $\gamma + \gamma$ and jet can be a light or a heavy flavor jet;

(ii) Higgs boson production from gluon-gluon fusion process; $pp \to H \to \gamma + \gamma$;

(iii) Higgs boson production in association with a vector boson; $pp \to H + V \to \gamma + \gamma +$jets, where $V = W^\pm$ and Z;

(iv) Diphoton production associated with b-quark jets (b-jets $+ \gamma\gamma +$ jets);

(v) Diphoton production associated with c-quark jets (c-jets $+ \gamma\gamma +$ jets). This background arises from the production of a pair of photon, not coming from Higgs boson, accompanied by c-quark jets, where the c-jets are mistagged as b-jets;

(vi) Diphoton production associated with light flavor jets where light flavor jets are misidentified as b-jets.

To ensure sufficient statistics and obtain a more precise estimate of their contributions, the diphoton production associated with different types of jets, including b-quark jets, c-quark jets, and light flavor (nonbottom, noncharm) quark jets, is generated separately in the analysis. By generating these processes independently, it becomes possible to have an adequate number of events for each specific jet flavor and accurately estimate their individual contributions to the diphoton final state. This approach allows for a more comprehensive understanding of the impact of different jet flavors on the diphoton signal and helps in properly accounting for their respective backgrounds in the analysis.

IV. SIMULATION AND ANALYSIS STRATEGY

The SM background processes and signal events are generated using the MadGraph5_aMC@NLO event generator. Specifically, the Higgs boson production in association with a b-quark and a jet sample is obtained by merging the Higgs boson plus b-quark ($H + b$) sample and the Higgs boson plus b-quark plus jet ($H + b +$ jet) sample using the MLM merging prescription. By merging the samples, a comprehensive description of the Higgs boson production in association with a b-quark and a jet is achieved, allowing for accurate modelling and analysis of the signal and background processes.

After generating the samples, they undergo further simulation and modelling to account for various effects. First, the samples are passed through PYTHIA 8.3 [56], which handles parton showering, hadronization, and the decay of unstable particles. To account for the effects of the detector, the Delphes 3.5.0 package [57] is utilized, which simulates both CMS detector phase II card and the FCC-hh card. Delphes takes the generated particles as input and applies realistic detector response and resolution effects to the particles. For jet reconstruction, the anti-$k_{\rm t}$ algorithm [58] with a cone size parameter $R = 0.4$, implemented in the FastJet package [59], is employed. This algorithm clusters particles into jets based on their proximity in the detector. To identify and tag jets originating from b-quarks, b-tagging efficiency and misidentification rates are considered. The efficiency of b-tagging for a jet is $p_{\rm T}$ and η dependent. Additionally, misidentification rates for charm-jets and light-flavor jets are taken into account. For example, for the HL-LHC with CMS Phase II Delphes card, the b-tagging efficiency for a jet with $p_{\rm T} \in [40, 50]$ and $|\eta| \leq 1.8$ is set to 66.6%. The misidentification rate for the charm-jets is $p_{\rm T} - \eta$ dependent and for the light-flavor jets is flat. For a charm-jet with $p_{\rm T} \in [40, 50]$ and $|\eta| \leq 1.8$ the misidentification rate is 18.8% while it is 1.0% for light-flavor jets independent of p_T and η. These rates reflect the likelihood of mistakenly tagging a charm-jet or a light-flavor jet as a b-jet. By incorporating these simulation and modeling steps, the analysis aims to realistically account for detector effects, jet reconstruction, and the identification of b-jets, charm-jets, and light-flavor jets, thereby providing a more accurate description of the experimental observables.

A. Events selection

To identify signal events, specific criteria are applied. The event selection requires the presence of exactly two isolated photons. These photons must have a transverse momentum greater than or equal to 20 GeV and a pseudorapidity within the range of $|\eta_{\gamma_{1,2}}| \leq 3.0$. An isolated photon is defined as one that exhibits minimal activity in its vicinity, reducing the probability of originating from a jet. A small value of the isolation variable indicates a high degree of isolation, implying that the photon is more likely to be a genuine rather than originating from a jet. The isolation of a photon, I_γ, is quantified using an isolation variable, which is calculated as the ratio of the sum of transverse momenta (p_T) of other particles around the photon to the transverse momentum of the photon itself. For both photons the isolation variable is required to be less than 0.15.

Additionally, each event must contain at least one jet, out of which at least one must be identified as b-jets using a b-tagging criterion. The jets (b-jets) are required to have a p_T greater than or equal to 30 GeV and a pseudorapidity within the range of $|\eta| \leq 4.0(3.0)$.

To ensure that the selected objects are well-isolated, an angular separation criterion is applied. The angular separation between any two objects (photons or jets) is quantified using the variable $\Delta R_{i,j} = \sqrt{(\eta_i - \eta_j)^2 + (\phi_i - \phi_j)^2}$, where ϕ represents the azimuthal angle and η represents the pseudorapidity. The requirement is set at $\Delta R_{i,j} \geq 0.4$ for all possible combinations of objects (photon-photon, photon-jet, and jet-jet). This criterion helps to ensure that the selected objects are sufficiently separated from each other in the detector.

By applying these selection criteria, the analysis aims to isolate signal events that satisfy the specific kinematic and isolation requirements, ensuring the quality and reliability of the data used for further analysis. Table I displays the efficiencies of the signal when the coupling c_b is set to 1.05 and the coupling $\tilde{c}_b$ is set to 0.0. It also includes the efficiencies of the main background processes after applying the cuts. The efficiencies represent the fraction of events that pass the selection criteria, for each process.

The cross sections of other background processes such as H, HZ, and HW after the selection are found to be negligible in both HL-LHC and FCC-hh. At the end of this section, we address the potential impact of a background arising from the misidentification of jets as photons in multijet and jets $+ \gamma$ production. This occurs when jets contain neutral pions that decay into two photons, resulting in overlapping photon showers that appear as a single photon in the detector. To mitigate the QCD multijet background, it is crucial to develop methods to identify and reject jets mimicking photons. This background process has a significantly higher cross section compared to other backgrounds, with a difference spanning several orders of magnitude. However, by applying kinematic requirements (excluding criteria related to photons) and ensuring the presence of only b-jets, the cross section of the multijet and jets $+ \gamma$ background is reduced to approximately 10^4 pb. The probability of a jet being misidentified as a photon depends on the transverse momentum of the fake photon, typically ranging from 10^{-5} to 10^{-3} depending on fake photons p_T. By imposing a requirement of two photons, the contribution of this background is effectively minimized to a low level. While this analysis neglects the multijet background, it is important to emphasise that a dedicated and more realistic detector simulation is necessary to accurately estimate its potential contribution. Such a simulation should consider the specific characteristics of the experimental setup and incorporate a detailed representation of the detector response. Future studies should address this aspect to provide a more comprehensive assessment of the multijet background's impact.

B. Multivariate analysis

In this analysis, the applied cuts on individual variables are generally loose, meaning they do not significantly suppress a substantial fraction of background events while also reducing the signal events. To achieve a better discrimination between the signal and background processes a multivariate analysis is used [60–64]. In particular a boosted decision tree (BDT) is trained to increase the sensitivity. All the backgrounds are taken into account during the BDT training, with each background process weighted accordingly. This helps in obtaining an effective

TABLE I. The efficiencies of the signal with $c_b = 1.05, \tilde{c}_b = 0.0$ and for the main SM background processes after applying the selection criteria.

	Signal	SM $H + b +$ jets	b-jets $+ \gamma\gamma$	c-jets $+ \gamma\gamma$	light-jets $+ \gamma\gamma$
HL-LHC	3.6%	3.4%	5.1%	0.25%	0.05%
FCC-hh	4.3%	4.1%	2.7%	0.58%	0.09%

separation of signal events from the background events. To enhance sensitivity, separate analyses are conducted for the *CP*-even and *CP*-odd signals using distinct BDT test and training sets. This approach allows for a more targeted investigation of each signal, optimizing the discrimination power and enhancing the overall sensitivity of the analysis. Distinct sets of variables for *CP*-even (c_b) and *CP*-odd ($\tilde{c}_b$) signal processes are employed in the BDT models for analyses at both the HL-LHC and FCC-hh. The included variables are as follows:

(i) $p_{T,\gamma_1}, p_{T,\gamma_2}$: transverse momenta of first and second photon;

(ii) $p_{T,\mathrm{b-jet}}$: transverse momentum of the most energetic b-jet;

(iii) $p_{T,\gamma_1\gamma_2} = |\vec{p}_{T,\gamma_1} + \vec{p}_{T,\gamma_2}|$: the magnitude of the vector sum of the transverse momenta of the two photons;

(iv) $M_{\gamma_1\gamma_2}$: invariant mass of two photons (reconstructed Higgs boson mass);

(v) $M_{\gamma_1,\gamma_2,\mathrm{b-jet}}$: the invariant mass of two photons and the leading b-jet system;

(vi) $M_{\gamma_1,\mathrm{b-jet}}$: the invariant mass of leading photon and leading b-jet system;

(vii) $M_{\gamma_2,\mathrm{b-jet}}$: the invariant mass of second photon and first leading b-jet system;

(viii) $\Delta R(\gamma_1,\gamma_2)$: the angular distance between the first and second photon;

(ix) $\cos(\gamma_1,\gamma_2)$: the cosine of angle between the two photons;

(x) $\Delta\phi(\gamma_{1,2}, \mathrm{b-jet})$: the azimuthal angle between the photons and the b-jet. These azimuthal angle variables are expected to be sensitive to the *CP*-violating coupling [65–68];

(xi) Mean IP of the b-tagged jet defined as follows:

$$\frac{\sum_{\mathrm{i=trk}}^{N_{\mathrm{trk}}} \sqrt{d_{0,i}^2 + d_{z,i}^2}}{N_{\mathrm{trk}}}, \tag{6}$$

where $d_{0,i}$ and d_z, i are the transverse impact parameter and the longitudinal impact parameter values of ith track inside the b-tagged jet cone with $\Delta R = 0.4$. The total number of tracks inside the jet cone is N_{trk};

(xii) b-jet charge ($\mathbf{Q}_{\mathrm{b-jet}}$);

$$\frac{\sum_i q_i \times p_{T,i}}{p_{T,\mathrm{b-jet}}}, \tag{7}$$

where the sum is over the particles inside the reconstructed b-jet cone, q_i is the integer charge value of the observed color-neutral object, $p_{\mathrm{T,i}}$ is the magnitude of its transverse momentum with respect

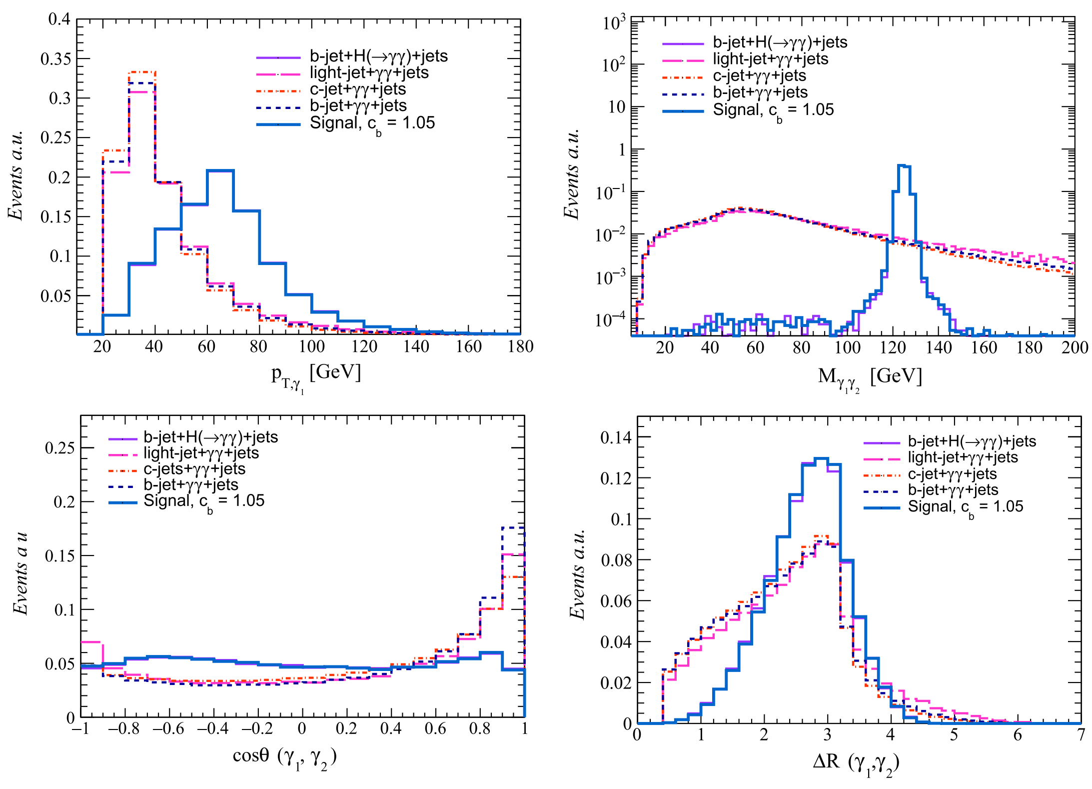

FIG. 2. Normalized distributions for the signal with $c_b = 1.05$, $\tilde{c}_b = 0.0$ and the main background processes of some of the input variables at the HL-LHC used in the BDT after the selection criteria. In particular, first photon p_T, invariant mass of diphoton, cosine of the angle between two photons [$\cos(\gamma_1,\gamma_2)$], and the angular distance between the diphoton system [$\Delta R(\gamma_1,\gamma_2)$].

to the beam axis, and the total transverse momentum of the b-jet is denoted by $p_{\mathrm{T,b-jet}}$. More details of the jet charge definition is found Ref. [69].

Figure 2 displays the normalized distributions of some the input variables for the CP-even signal. The distributions for signal are for the case $c_b = 1.05$, $\tilde{c}_b = 0.0$. In particular, first photon p_T, invariant mass of diphoton, cosine of the angle between two photons [$\cos(\gamma_1, \gamma_2)$], and the angular distance between the diphoton system [$\Delta R(\gamma_1, \gamma_2)$] are depicted in Fig. 2. The normalized distributions of some the input variables for the CP-odd case with $c_b = 1.0$, $\tilde{c}_b = 0.1$ as for signal events are presented in Fig. 3. The invariant mass of the leading photon and the leading jet system, highest p_T b-jet, and the difference between the azimuthal angles of $\gamma_{1,2}$ and the p_T of the highest p_T b-jet are shown as examples of the input variables for the CP-odd BDT.

There is a substantial contribution from the c-jet $+ \gamma\gamma +$ jets background, primarily arising from the elevated misidentification rate of c-quark jets as b-jets. This misattribution is rooted in the reliance of heavy-flavor jet identification algorithms on variables linked to the characteristics of heavy-flavor hadrons, such as their lifetimes. Notably, heavy-flavor hadrons containing b-quarks exhibit a lifetime on the order of 1.5 ps, whereas c-hadrons have a lifetime of 1 ps or less. Consequently, b-hadrons typically display displacements ranging from a few millimeters to one centimeter, depending on their momentum-values that can align with those of energetic jets containing c-hadrons. To discern between backgrounds featuring jets originating from c quarks, we utilize the mean impact parameter and the charge of the identified b-jet as input variables for the BDT. The distribution of these two variables for the b-jet $+ H(\to\gamma\gamma) +$ jets and the c-jet $+ \gamma\gamma +$ jets backgrounds is illustrated in Fig. 4 for comparative analysis.

It is notable that there is always room for improvement in the analysis, especially by selecting a more optimal set of variables. However, the variables utilized in our study have proven to be effective discriminators, as evidenced below. We employ the relative importance to filter out the most crucial variables while maintaining the accuracy of the BDT. By utilizing the feature importance, we identify and retain the variables that have the highest significance without compromising the overall accuracy of the BDT model. The mean IP, b-jet charge, and the invariant mass of the diphoton system, and the cosine between the two photons angle emerge as the most significant in distinguishing the signal from the backgrounds for both the HL-LHC and FCC-hh. In Fig. 5, we present the relative importance of each observable based on the separation between the signal and backgrounds. The ranking is shown for both the

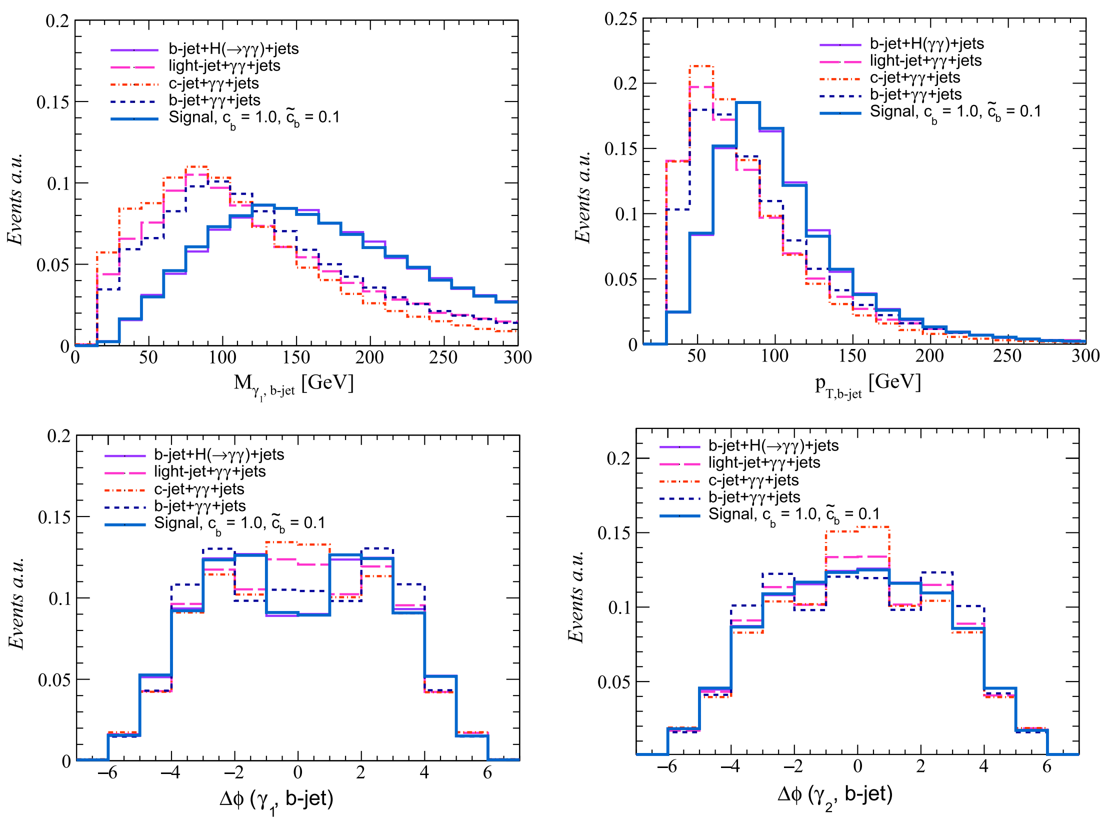

FIG. 3. Normalized distributions for the CP-odd signal events with $c_b = 1.0$, $\tilde{c}_b = 0.1$ and the main background processes of some of the input variables at the HL-LHC used in the BDT after the selection criteria. The invariant mass of the leading photon and the leading jet system ($M_{\gamma_1,\mathrm{b-jet}}$), leading b-jet p_T, and the difference between the azimuthal angles of $\gamma_{1,2}$ and the leading b-jet [$\Delta\phi(\gamma_{1,2}, \mathrm{b-jet})$].

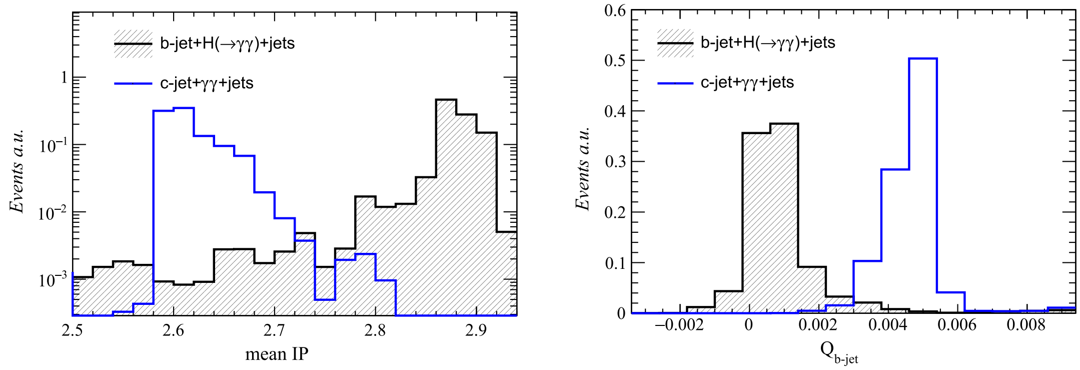

FIG. 4. Normalized mean IP and $Q_{\text{b-jet}}$ distributions for the b-jet $+ H(\rightarrow \gamma\gamma) +$ jets and the c-jet $+ \gamma\gamma +$ jets background. The definitions of mean IP and $Q_{\text{b-jet}}$ are given in Eqs. (6) and (7), respectively.

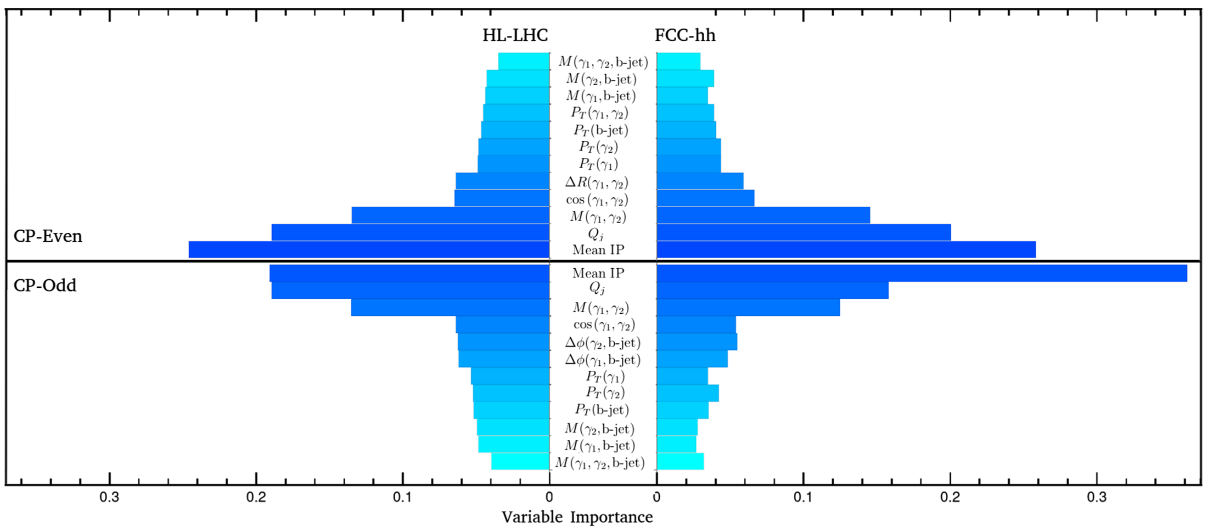

FIG. 5. Input kinematic variables for the BDT and their significance in distinguishing the CP-even signal (top) and CP-odd signal (bottom). On the left, variable importance is illustrated for the LHC, while the right-side plot showcases the same analysis for the FCC-hh.

HL-LHC and the FCC-hh. The top panel illustrates the relevance of kinematic variables as inputs for the BDT in distinguishing CP-even signals, while the bottom panel focuses on CP-odd signals from the main background processes. The left subplot depicts variable importance for the LHC, and the right subplot presents the corresponding analysis for the FCC-hh.

We proceed with the implementation of the BDT algorithm using the following methodology. The datasets containing independent event samples for both the signal and background are randomly divided into two equal parts. One part is used to train the BDT algorithm, while the other serves as a validation set for both signal and background events.

As mentioned earlier, we employ twelve parameters to train the BDT algorithm separately for CP-even and CP-odd. To ensure optimal performance and minimise the risk of overtraining, we take necessary precautions. We have taken explicit measures to prevent overtraining by verifying that the Kolmogorov-Smirnov probability, which measures the similarity between distributions. Figure 6 displays that BDT output distributions for both HL-LHC (top) and FCC-hh (bottom) and illustrates the Kolmogorov-Smirnov probability for both the training and testing samples, demonstrating that neither the signal nor the background samples are overtrained. To optimise sensitivity, we apply an appropriate cut on the BDT response. This cut is determined to maximise the ability to discriminate between the signal and background events. By applying this cut, we obtain the corresponding numbers of signal ($\mathbf{N}_\mathrm{S}$) and background ($\mathbf{N}_\mathrm{B}$) events. Using these event counts, we calculate the sensitivity for parameters c_b and $\tilde{c}_b$.

V. RESULTS

To determine the statistical significance, denoted as $\mathcal{S}$, we employ the following formula. Given a number of

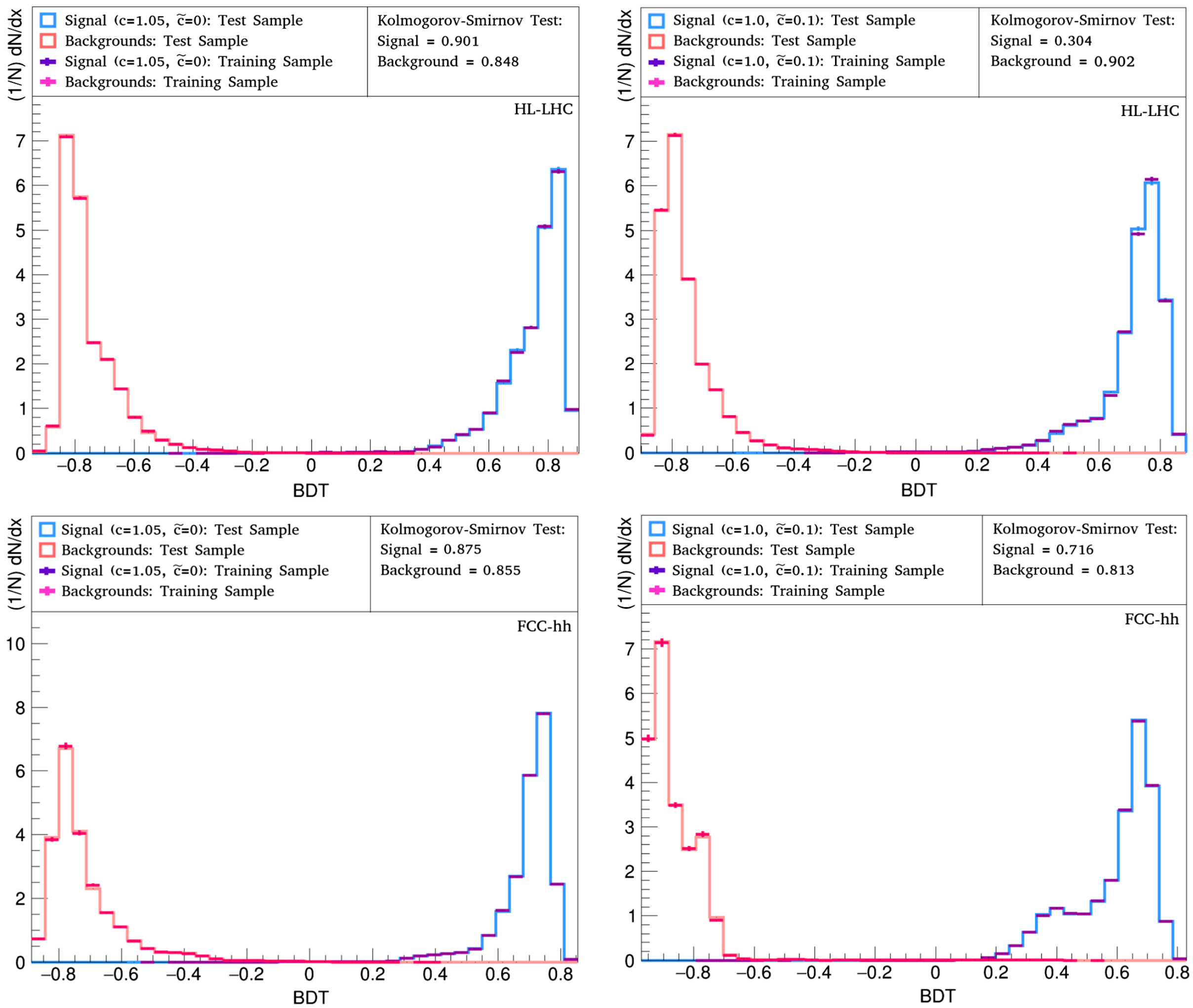

FIG. 6. The normalized BDT output distributions for signal and background at HL-LHC (top) and FCC-hh (bottom). The distributions are presented for the CP-even scenario with $(c_b = 1.05, \tilde{c}_b = 0.0)$ (left) and the CP-odd case with $(c_b = 1.0, \tilde{c}_b = 0.1)$ (right). The Kolmogorov-Smirnov probabilities are given in the plots as well.

signal events ($\mathbf{N}_\mathrm{S}$) and background events ($\mathbf{N}_\mathrm{B}$) at a specific luminosity ($\mathcal{L}$), considering an uncertainty of Δ_B on background, the significance ($\mathcal{S}$) is calculated as [70,71]

$$\mathcal{S} = \left[2 \times \left((\mathbf{N}_\mathrm{S} + \mathbf{N}_\mathrm{B}) \ln\left[\frac{(\mathbf{N}_\mathrm{S} + \mathbf{N}_\mathrm{B})(\mathbf{N}_\mathrm{B} + \Delta_\mathrm{B}^2)}{\mathbf{N}_\mathrm{B}^2 + (\mathbf{N}_\mathrm{S} + \mathbf{N}_\mathrm{B})\Delta_\mathrm{B}^2}\right] - \frac{\mathbf{N}_\mathrm{B}^2}{\Delta_\mathrm{B}^2} \ln\left[1 + \frac{\Delta_\mathrm{B}^2 \times \mathbf{N}_\mathrm{S}}{\mathbf{N}_\mathrm{B}(\mathbf{N}_\mathrm{B} + \Delta_\mathrm{B}^2)}\right]\right)\right]^{1/2}. \tag{8}$$

In case that $\Delta_\mathrm{B} = 0$, $\mathcal{S}$ is reduced to the following formula:

$$\mathcal{S} = \sqrt{2 \times \left[(\mathbf{N}_\mathrm{S} + \mathbf{N}_\mathrm{B}) \ln\left(1 + \frac{\mathbf{N}_\mathrm{S}}{\mathbf{N}_\mathrm{B}}\right) - \mathbf{N}_\mathrm{S}\right]}. \tag{9}$$

In the limit of large number of background events with respect to signal, $\mathcal{S} = \mathbf{N}_\mathrm{S}/\sqrt{\mathbf{N}_\mathrm{B}}$. Now, we present the sensitivity reach for both the HL-LHC and the FCC-hh. In Fig. 7, the 1σ and 2σ allowed regions for c_b and $\tilde{c}_b$ are displayed in Table II and Fig. 7. The integrated luminosity considered for the HL-LHC is 3 ab^{-1}, while for the FCC-hh, it is taken as 15 ab^{-1}. The regions allowed within 1σ and 2σ are also displayed, accounting for a systematic uncertainty of 25% for background.

A. Bounds on $(c_b, \tilde{c}_b)$ space

Figure 8 illustrates the anticipated 1σ exclusion regions within the $c_b - \tilde{c}_b$ parameter space for both the HL-LHC and FCC-hh colliders, taking into account integrated luminosities of 3 ab^{-1} and 15 ab^{-1}, respectively. These exclusion limits were calculated under the assumption that the kinematics of the signal events remain independent of the specific values of the c_b and $\tilde{c}_b$ couplings. Additionally, the presented limits incorporate an overall systematic uncertainty of 25%. Upon comparison, it is evident that

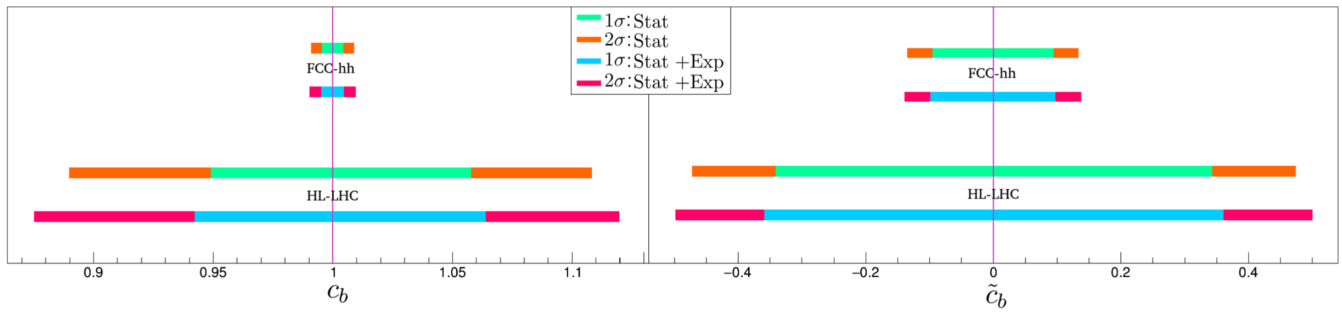

FIG. 7. The 1σ and 2σ regions for c_b and $\tilde{c}_b$ by considering only statistical uncertainty and statistical uncertainty plus 25% overall systematic uncertainty at the HL-LHC and FCC-hh.

the limits experience slight enhancements with the increase in center-of-mass energy from the HL-LHC to the FCC-hh. The parameter space region obtained for the FCC-hh exhibits a circular shape, similar to that for the HL-LHC. However, due to the compactness of the region delineated for the FCC-hh, we opted to zoom in on a restricted area surrounding the SM value. Consequently, this adjustment resulted in an elliptical appearance, facilitating a more refined visualization of the parameter space vicinity to the SM point.

VI. EXPLORATION OF THE $Hb\bar{b}$ CP-ODD COUPLING

In this section, we introduce an asymmetry observable that is sensitive to the magnitude of the pseudoscalar coupling ($\tilde{c}_b$). To evaluate this observable, we apply the simulation chain and selection criteria described in Sec. IV for various values of the $\tilde{c}_b$ coupling.

The differential production cross section associated to any CP-mixed case of the $Hb\bar{b}$ coupling in $\mathrm{H}+\mathrm{b}+\mathrm{jet}$ signal can be parametrized according to the following:

$$d\sigma = c_b^2 \times d\sigma_{CP-\mathrm{even}} + \tilde{c}_b^2 \times d\sigma_{CP-\mathrm{odd}} + c_b \times \tilde{c}_b \times d\sigma_{\mathrm{int}}, \quad (10)$$

where $d\sigma_{CP-\mathrm{even}}$, $d\sigma_{CP-\mathrm{odd}}$, and $d\sigma_{\mathrm{int}}$ are corresponding to the signal differential cross sections for the CP-even, CP-odd couplings and interference terms, respectively. The integration of the interference term in Eq. (10) over the whole phase space disappears because when a CP-even amplitude and a CP-odd amplitude interfere, the resulting interference term oscillates in sign across different regions of phase space and the integral of an odd function over a symmetric interval vanishes. Consequently, the interference term doesn't add anything to the overall rate or to CP-even measurements like transverse momenta and invariant masses distributions. Instead, it only affects observables designed specifically to measure CP-odd phenomena. We construct an asymmetry observable from the azimuthal angular distributions of the final state objects in $pp \to H(\to \gamma\gamma) + b + j$ process. This observable, $\mathcal{O}_\phi$, is sensitive to the CP-violating $\tilde{c}_b$ coupling of the $Hb\bar{b}$ interaction. We define the angular asymmetry $\mathcal{O}_\phi$ with respect to the azimuthal angle as

$$\mathcal{O}_\phi = \frac{N^+ - N^-}{N^+ + N^-}, \quad (11)$$

where

$$N^+ = \int_0^\pi \frac{dN}{d\Delta\phi(H,b)}, \quad \text{and} \quad N^- = \int_{-\pi}^0 \frac{dN}{d\Delta\phi(H,b)}, \quad (12)$$

where $\Delta\phi(H,b)$ is defined as the azimuthal angle between the Higgs boson and the highest p_T b-quark in the event,

TABLE II. The expected 1σ and 2σ limits on c_b and $\tilde{c}_b$ couplings considering only statistical uncertainty and statistical uncertainty plus 25% overall systematic uncertainty at the HL-LHC and FCC-hh with the integrated luminosity of 3 ab^{-1} and 15 ab^{-1}.

$c_b/\tilde{c}_b$	$1\sigma/2\sigma$	Uncertainty	HL-LHC	FCC-hh
$c_b(\tilde{c}_b = 0)$	1σ	Statistical	$[-1.057, -0.948] \cup [0.949, 1.057]$	$[-1.0045, -0.995] \cup [0.995, 1.0045]$
		Stat $\oplus$ Syst	$[-1.063, -0.940] \cup [0.941, 1.064]$	$[-1.0048, -0.996] \cup [0.996, 1.0048]$
	2σ	Statistical	$[-1.107, -0.889] \cup [0.889, 1.108]$	$[-1.009, -0.990] \cup [0.990, 1.009]$
		Stat $\oplus$ Syst	$[-1.120, -0.873] \cup [0.873, 1.120]$	$[-1.010, -0.991] \cup [0.991, 1.010]$
$\tilde{c}_b(c_b = 1)$	1σ	Statistical	$[-0.33, 0.33]$	$[-0.069, 0.069]$
		Stat $\oplus$ Syst	$[-0.35, 0.35]$	$[-0.072, 0.072]$
	2σ	Statistical	$[-0.46, 0.46]$	$[-0.097, 0.097]$
		Stat $\oplus$ Syst	$[-0.49, 0.49]$	$[-0.101, 0.101]$

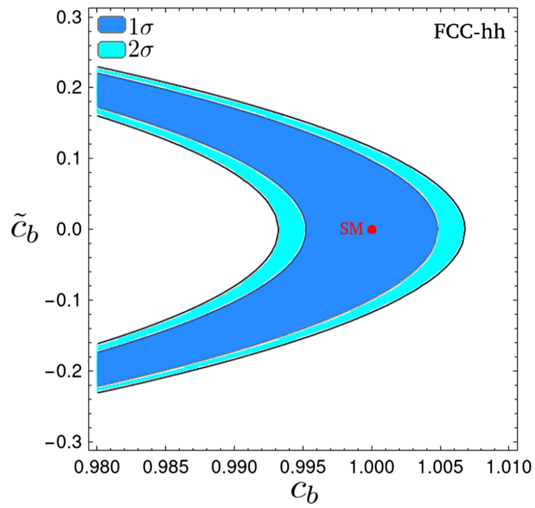

FIG. 8. Expected 2σ regions in the c_b-$\tilde{c}_b$ plane obtained for the HL-LHC and FCC-hh with the integrated luminosities of 3 ab^{-1} and 15 ab^{-1}, respectively. The limits are derived assuming an overall uncertainty of 25% on the background estimation. The red circle indicates the SM.

where the Higgs boson is reconstructed from the two photons. According to the general expression provided in Eq. (10), we anticipate the following functional form for the asymmetry:

$$\mathcal{O}_\phi(c_b, \tilde{c}_b) = \frac{A \times c_b^2 + B \times \tilde{c}_b^2 + C \times c_b \tilde{c}_b}{D \times c_b^2 + E \times \tilde{c}_b^2}, \quad (13)$$

where $\mathcal{O}_\phi(c_b = 1.0, \tilde{c}_b = 0.0)$ is the SM case. We note that the denominator represents the total cross section and thus does not contain an interference term. Assuming $c_b = 1.0$, the deviation of $\mathcal{O}_\phi$ due to the CP-odd coupling from the SM has the following form:

$$\begin{aligned} \delta\mathcal{O}_\phi(\tilde{c}_b) &= \mathcal{O}_\phi(c_b = 1.0, \tilde{c}_b) - \mathcal{O}_\phi(c_b = 1.0, \tilde{c}_b = 0.0) \\ &= \frac{B' \times \tilde{c}_b^2 + C' \times \tilde{c}_b}{1.0 + E' \times \tilde{c}_b^2}, \end{aligned} \quad (14)$$

where parameters $B' \equiv (BD - AE)/D^2$, $C' \equiv C/D$, and $E' \equiv E/D$. To illustrate the sensitivity of the asymmetry, we explore the relationship between the $\delta\mathcal{O}_\phi$ and $\tilde{c}_b$ coupling. Several Monte Carlo simulated samples consisting of 500 K events is analyzed to discern the degree to which the asymmetry is influenced by the presence of the $\tilde{c}_b$ coupling. The difference between the asymmetry and its SM value, $\delta\mathcal{O}_\phi$, is plotted against $\tilde{c}_b$ at the LHC, as illustrated in Fig. 9. In the plot, the value of c_b is fixed at the SM value of 1.0 and the uncertainty depicted is purely statistical. By conducting a fit, we derive the following result: $B' = -0.09 \pm 0.003$, $C' = 0.0006 \pm 0.0005$, and $E' = 2.9 \pm 0.3$. It is evident from the plot that the $\mathcal{O}_\phi$ exhibits sensitivity to the magnitude of CP-odd coupling. As $|\tilde{c}_b|$ increases, $\delta\mathcal{O}_\phi$ falls below the SM value. It is noteworthy that $\delta\mathcal{O}_\phi$ receives a minor impact from the interference term because of the very small coefficient of linear term of $\tilde{c}_b$ with respect to the term $\tilde{c}_b^2$, i.e., $|C'| \ll |B'|$. As a result, the bounds which will be derived on $\tilde{c}_b$ using $\mathcal{O}_\phi$ are expected to exhibit only a minimal degree of asymmetry.

We also investigate the sensitivity of the asymmetry as a probe of CP-violating couplings at the HL-LHC and FCC-hh. To quantify this, all selection criteria presented in Sec. IVA are followed. We assess the statistical significance in the measurement of the asymmetry $\mathcal{O}_\phi$ as $S_{\mathcal{O}_\phi} = \mathcal{O}_\phi/\Delta\mathcal{O}_\phi$, where $\Delta\mathcal{O}_\phi$ is

$$\Delta\mathcal{O}_\phi = \sqrt{\frac{1 - \mathcal{O}_\phi^2}{\sigma_{\rm SM} \times \mathcal{L}}}, \quad (15)$$

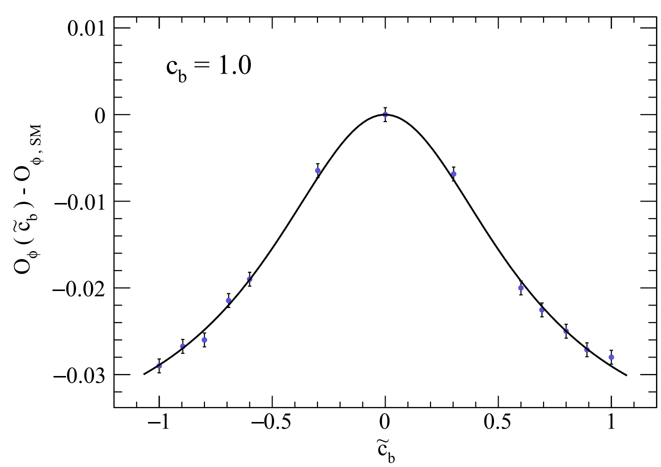

FIG. 9. The variation of the asymmetry from its SM prediction is examined by plotting the difference $\delta\mathcal{O}_\phi$ as defined in Eq. (14). This variation is analyzed as a function of $\tilde{c}_b$ at the LHC. The uncertainty is pure statistical.

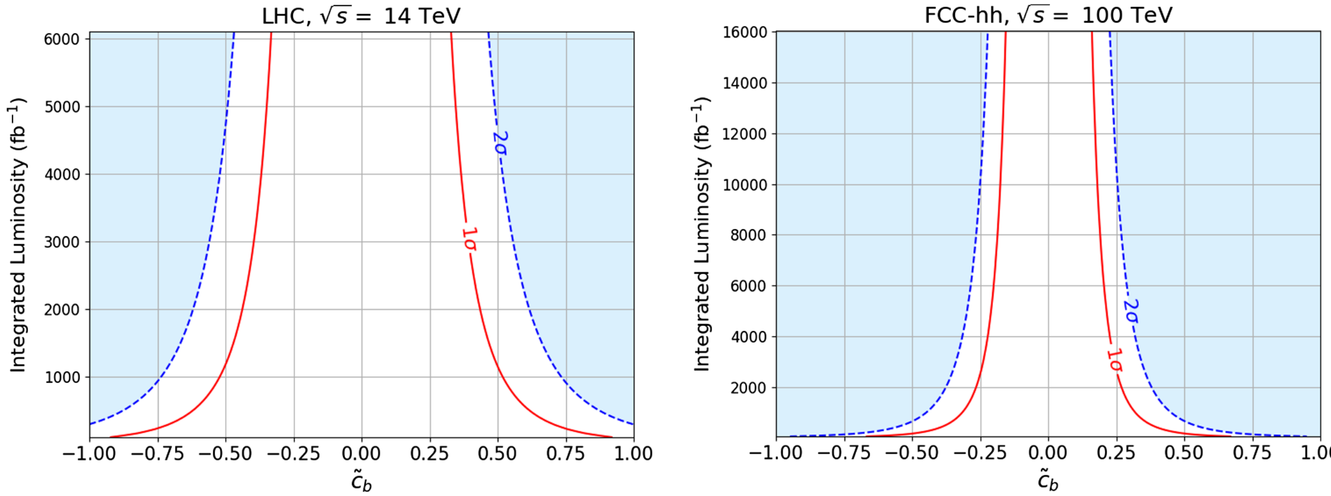

FIG. 10. The 1σ and 2σ regions versus the integrated luminosity for $\tilde{c}_b$ for the HL-LHC (left) and FCC-hh (right). The regions are obtained considering only statistical uncertainty.

where $\sigma_{\rm SM}$ is the SM cross section and $\mathcal{L}$ is the integrated luminosity. The signal significance $S_{\mathcal{O}_\phi}$ is dependent on c_b and $\tilde{c}_b$ and has the following form:

$$S_{\mathcal{O}_\phi}(c_b, \tilde{c}_b) = \frac{\mathcal{O}_\phi - \mathcal{O}_{\phi,\rm SM}}{\sqrt{1 - \mathcal{O}^2_{\phi,\rm SM}}} \times \sqrt{\sigma_{\rm SM} \times \mathcal{L}}. \qquad (16)$$

As our focus lies on the CP-odd coupling, c_b is set to its SM value and we concentrate on $\tilde{c}_b$. In Fig. 10, the 1σ and 2σ regions of $\tilde{c}_b$ are depicted versus the integrated luminosity for both the HL-LHC and FCC-hh.

As observed, the 1σ (2σ) region of $\tilde{c}_b$ is accessible down to $-0.40 \leq \tilde{c}_b \leq 0.38(-0.62 \leq \tilde{c}_b \leq 0.61)$ with an integrated luminosity of 3000 fb^{-1} at the HL-LHC and down to $[-0.16 \leq \tilde{c}_b \leq 0.15(-0.23 \leq \tilde{c}_b \leq 0.22)]$ with an integrated luminosity of 15000 fb^{-1} at the FCC-hh.

VII. SUMMARY AND CONCLUSIONS

This study focused on investigating the sensitivity of the $H + b +$ jets process at the HL-LHC and FCC-hh colliders in order to explore the CP-even and CP-odd couplings of $Hb\bar{b}$. The analysis involved constraining the new physics couplings, c_b and $\tilde{c}_b$, by conducting a search through the $H + b +$ jets channel and studying the subsequent decay of the Higgs boson into two photons. Monte Carlo event generation was employed to simulate the signal and relevant background processes, and detector effects were taken into account. To distinguish the signal from the background, a carefully selected set of discriminating variables was analyzed using a multivariate technique, in particular, by employing BDTs. The expected 1σ and 2σ limits on c_b and $\tilde{c}_b$ were obtained, and the exclusion region in the $c_b - \tilde{c}_b$ plane were determined. These limits correspond to integrated luminosities of 3 ab^{-1} and 15 ab^{-1} for the HL-LHC and FCC-hh, respectively.

Comparing the obtained limits with the current experimental bounds, it was found that a significant portion of the unexplored $c_b - \tilde{c}_b$ parameter space could be accessed through this analysis. By assuming one nonzero coupling at a time for comparison, the c_b coupling was found to range from $[-1.2, -1.17] \cup [0.88, 1.12]$ based on the LHC Higgs signal strength data at 90% CL. The direct predicted ranges from this study were $[-1.12, -0.873] \cup [0.873, 1.12]$ for the HL-LHC and $[-1.010, -0.991] \cup [0.991, 1.010]$ for the FCC-hh.

Regarding the $\tilde{c}_b$ parameter, the current limits were within the range $[-0.5, 0.5]$ based on the LHC Higgs signal strength data and $[-0.26, 0.26]$ from electron EDM at 90% CL. The direct measurement from this analysis excluded the range $[-0.49, 0.49]$ for the HL-LHC and $[-0.10, 0.10]$ for the FCC-hh at the 2σ level. Both the HL-LHC and FCC-hh demonstrated the potential to provide limits on c_b and $\tilde{c}_b$ at the same order of magnitude as or even better than those obtained from indirect bounds.

We also introduced a novel asymmetry tailored to investigate CP violation within the $Hb\bar{b}$ coupling, applying exclusively lab-frame momenta. Our analysis underscored the effectiveness of this asymmetry in constraining the CP-odd couplings of the bottom quark Yukawa couplings.

Upon contrasting the findings of this study, it becomes apparent that the $H + b +$ jets process emerges as a powerful and direct avenue for investigating both the CP-even and CP-odd aspects of the $Hb\bar{b}$ interactions at proton-proton colliders. This efficacy is primarily attributed to the incorporation of a more extensive final state. There are potential avenues to improve the results. Firstly, incorporating complete next-to-leading order predictions for the $H + b +$ jet process, including loop level diagrams, can yield more accurate and reliable outcomes. Secondly, to enhance sensitivity and statistical significance, the inclusion of additional decay modes of the Higgs boson, such as WW and ZZ needs to be considered.

ACKNOWLEDGMENTS

The authors would like to thank M. Ebrahimi for her fruitful discussions in multivariate analysis algorithms and M. Zaro for his valuable guidances in generating events with MadGraph.

[1] M. Aaboud *et al.* (ATLAS Collaboration), Phys. Lett. B **786**, 59 (2018).
[2] A. M. Sirunyan *et al.* (CMS Collaboration), Phys. Rev. Lett. **121**, 121801 (2018).
[3] G. Aad *et al.* (ATLAS Collaboration), Eur. Phys. J. C **81**, 178 (2021).
[4] The CMS Collaboration, Report No. CMS-PAS-FTR-18-011, CERN, https://inspirehep.net/literature/1703974.
[5] Y. Heo, D. W. Jung, and J. S. Lee, arXiv:2402.02822.
[6] S. Heinemeyer *et al.* (LHC Higgs Cross Section Working Group Collaboration), arXiv:1307.1347.
[7] A. Tumasyan *et al.* (CMS Collaboration), Nature (London) **607**, 60 (2022).
[8] M. Cepeda, S. Gori, P. Ilten, M. Kado, F. Riva, R. Abdul Khalek, A. Aboubrahim, J. Alimena, S. Alioli, A. Alves *et al.*, CERN Yellow Rep. Monogr. **7**, 221 (2019).
[9] A. Crivellin, Proc. Sci. DISCRETE2022 (**2024**) 006 [arXiv:2304.01694].
[10] K. G. Wilson, Rev. Mod. Phys. **55**, 583 (1983).
[11] T. Appelquist and J. Carazzone, Phys. Rev. D **11**, 2856 (1975).
[12] W. Buchmuller and D. Wyler, Nucl. Phys. **B268**, 621 (1986).
[13] B. Grzadkowski, M. Iskrzynski, M. Misiak, and J. Rosiek, J. High Energy Phys. 10 (**2010**) 085.
[14] K. Hagiwara, S. Ishihara, R. Szalapski, and D. Zeppenfeld, Phys. Rev. D **48**, 2182 (1993).
[15] C. N. Leung, S. T. Love, and S. Rao, Z. Phys. C **31**, 433 (1986).
[16] M. B. Einhorn and J. Wudka, Nucl. Phys. **B876**, 556 (2013).
[17] S. Willenbrock and C. Zhang, Annu. Rev. Nucl. Part. Sci. **64**, 83 (2014).
[18] R. Contino, M. Ghezzi, C. Grojean, M. Muhlleitner, and M. Spira, J. High Energy Phys. 07 (2013) 035.
[19] S. Bar-Shalom, A. Soni, and J. Wudka, Phys. Rev. D **92**, 015018 (2015).
[20] R. S. Gupta, A. Pomarol, and F. Riva, Phys. Rev. D **91**, 035001 (2015).
[21] A. Alloul, B. Fuks, and V. Sanz, J. High Energy Phys. 04 (2014) 110.
[22] F. Bishara, P. Englert, C. Grojean, G. Panico, and A. N. Rossia, J. High Energy Phys. 06 (2023) 077.
[23] H. Bahl, E. Fuchs, S. Heinemeyer, J. Katzy, M. Menen, K. Peters, M. Saimpert, and G. Weiglein, Eur. Phys. J. C **82**, 604 (2022).
[24] J. Brod, J. M. Cornell, D. Skodras, and E. Stamou, J. High Energy Phys. 08 (2022) 294.
[25] A. Djouadi and G. Moreau, Eur. Phys. J. C **73**, 2512 (2013).
[26] R. Harnik, A. Martin, T. Okui, R. Primulando, and F. Yu, Phys. Rev. D **88**, 076009 (2013).
[27] F. Bishara, Y. Grossman, R. Harnik, D. J. Robinson, J. Shu, and J. Zupan, J. High Energy Phys. 04 (2014) 084.
[28] F. Demartin, B. Maier, F. Maltoni, K. Mawatari, and M. Zaro, Eur. Phys. J. C **77**, 34 (2017).
[29] H. Bahl and S. Brass, J. High Energy Phys. 03 (2022) 017.
[30] H. Bahl, P. Bechtle, S. Heinemeyer, J. Katzy, T. Klingl, K. Peters, M. Saimpert, T. Stefaniak, and G. Weiglein, J. High Energy Phys. 11 (2020) 127.
[31] J. Ellis, V. Sanz, and T. You, J. High Energy Phys. 07 (2014) 036.
[32] T. Corbett, O. J. P. Eboli, J. Gonzalez-Fraile, and M. C. Gonzalez-Garcia, Phys. Rev. D **86**, 075013 (2012).
[33] J. Ellis, V. Sanz, and T. You, J. High Energy Phys. 03 (2015) 157.
[34] C. Englert, Y. Soreq, and M. Spannowsky, J. High Energy Phys. 05 (2015) 145.
[35] C. Englert and M. Spannowsky, Phys. Lett. B **740**, 8 (2015).
[36] J. A. Aguilar-Saavedra, J. M. Cano, and J. M. No, Phys. Rev. D **103**, 095023 (2021).
[37] T. Biswas and A. Datta, J. High Energy Phys. 05 (2023) 104.
[38] B. Carlson, T. Han, and S. C. I. Leung, Phys. Rev. D **104**, 073006 (2021).
[39] S. Khatibi and M. Mohammadi Najafabadi, Phys. Rev. D **90**, 074014 (2014).
[40] H. Khanpour, S. Khatibi, and M. Mohammadi Najafabadi, Phys. Lett. B **773**, 462 (2017).
[41] G. Haghighat, R. Jafari, H. Khanpour, and M. Mohammadi Najafabadi, arXiv:2305.05462.
[42] J. de Blas, M. Cepeda, J. D'Hondt, R. K. Ellis, C. Grojean, B. Heinemann, F. Maltoni, A. Nisati, E. Petit, R. Rattazzi *et al.*, J. High Energy Phys. 01 (2020) 139.
[43] E. Fuchs, M. Losada, Y. Nir, and Y. Viernik, J. High Energy Phys. 05 (2020) 056.
[44] C. Grojean, A. Paul, and Z. Qian, J. High Energy Phys. 04 (2021) 139.
[45] P. Konar, B. Mukhopadhyaya, R. Rahaman, and R. K. Singh, Phys. Lett. B **818**, 136358 (2021).
[46] F. Bordry, M. Benedikt, O. Brüning, J. Jowett, L. Rossi, D. Schulte, S. Stapnes, and F. Zimmermann, arXiv:1810.13022.
[47] C. Adolphsen, D. Angal-Kalinin, T. Arndt, M. Arnold, R. Assmann, B. Auchmann, K. Aulenbacher, A. Ballarino,

B. Baudouy and P. Baudrenghien *et al.*, CERN Yellow Rep. Monogr. **1**, 1 (2022).

[48] P. Artoisenet, P. de Aquino, F. Demartin, R. Frederix, S. Frixione, F. Maltoni, M. K. Mandal, P. Mathews, K. Mawatari, V. Ravindran *et al.*, J. High Energy Phys. 11 (2013) 043.

[49] V. Andreev *et al.* (ACME Collaboration), Nature (London) **562**, 355 (2018).

[50] J. Alwall, M. Herquet, F. Maltoni, O. Mattelaer, and T. Stelzer, J. High Energy Phys. 06 (2011) 128.

[51] J. Alwall, C. Duhr, B. Fuks, O. Mattelaer, D. G. Ozturk, and C. H. Shen, Comput. Phys. Commun. **197**, 312 (2015).

[52] J. Alwall, R. Frederix, S. Frixione, V. Hirschi, F. Maltoni, O. Mattelaer, H.-S. Shao, T. Stelzer, P. Torrielli, and M. Zaro, J. High Energy Phys. 07 (**2014**) 079.

[53] A. Alloul, N. D. Christensen, C. Degrande, C. Duhr, and B. Fuks, Comput. Phys. Commun. **185**, 2250 (2014).

[54] C. Degrande, C. Duhr, B. Fuks, D. Grellscheid, O. Mattelaer, and T. Reiter, Comput. Phys. Commun. **183**, 1201 (2012).

[55] M. L. Mangano, M. Moretti, F. Piccinini, and M. Treccani, J. High Energy Phys. 01 (2007) 013.

[56] T. Sjostrand, S. Ask, J. R. Christiansen, R. Corke, N. Desai, P. Ilten, S. Mrenna, S. Prestel, C. O. Rasmussen, and P. Z. Skands, Comput. Phys. Commun. **191**, 159 (2015).

[57] J. de Favereau, C. Delaere, P. Demin, A. Giammanco, V. Lemaître, A. Mertens, and M. Selvaggi (DELPHES 3 Collaboration), J. High Energy Phys. 02 (2014) 057.

[58] M. Cacciari, G. P. Salam, and G. Soyez, J. High Energy Phys. 04 (2008) 063.

[59] M. Cacciari, G. P. Salam, and G. Soyez, Eur. Phys. J. C **72**, 1896 (2012).

[60] A. Hocker *et al.*, Proc. Sci. ACAT2007 (**2007**) 040 [arXiv: physics/0703039].

[61] J. Stelzer, A. Hocker, P. Speckmayer, and H. Voss, Proc. Sci. ACAT2008 (**2008**) 063.

[62] J. Therhaag (TMVA Core Developer Team), AIP Conf. Proc. **1504**, 1013 (2009).

[63] P. Speckmayer, A. Hocker, J. Stelzer, and H. Voss, J. Phys. Conf. Ser. **219**, 032057 (2010).

[64] J. Therhaag, Proc. Sci. ICHEP2010 (**2010**) 510.

[65] C. Englert, P. Galler, A. Pilkington, and M. Spannowsky, Phys. Rev. D **99**, 095007 (2019).

[66] N. Mileo, K. Kiers, A. Szynkman, D. Crane, and E. Gegner, J. High Energy Phys. 07 (2016) 056.

[67] S. D. Rindani, P. Sharma, and A. Shivaji, Phys. Lett. B **761**, 25 (2016).

[68] F. Boudjema, R. M. Godbole, D. Guadagnoli, and K. A. Mohan, Phys. Rev. D **92**, 015019 (2015).

[69] D. Krohn, M. D. Schwartz, T. Lin, and W. J. Waalewijn, Phys. Rev. Lett. **110**, 212001 (2013).

[70] G. Cowan, K. Cranmer, E. Gross, and O. Vitells, Eur. Phys. J. C **71**, 1554 (2011); **73**, 2501(E) (2013).

[71] R. D. Cousins, J. T. Linnemann, and J. Tucker, Nucl. Instrum. Methods Phys. Res., Sect. A **595**, 480 (2008).